First-Principles Investigations on Structural, Elastic, and Thermodynamic Properties of Ce-La Alloys Under High Pressure

Li-Qin Zhang[a,b], Yan Cheng[a], Zhen-Wei Niu[a], and Guang-Fu Ji[c]

[a] Key Laboratory of High Energy Density Physics and Technology of Ministry of Education, College of Physical Science and Technology, Sichuan University, Chengdu 610064, China
[b] Department of Physics and Electronic Information, Huaibei Normal University, Huaibei 235000, China
[c] National Key Laboratory for Shock Wave and Detonation Physics Research, Institute of Fluid Physics, Chinese Academy of Engineering Physics, Mianyang 621900, China

Reprint requests to Y. C.; E-mail: ycheng@scu.edu.cn

Z. Naturforsch. **69a,** 52 – 60 (2014) / DOI: 10.5560/ZNA.2013-0069
Received April 30, 2013 / revised September 16, 2013 / published online November 21, 2013

The structural stability, thermodynamic, elastic, and electronic properties of cerium (Ce)-lanthanum (La) alloys were investigated for different Ce/La ratios under pressure by first-principles calculations using on-the-fly (OTF) pseudopotential and general gradient approximation (GGA). The ground-state properties of lanthanum and cerium obtained by minimizing the total energy agree favourably with other work. We derived the elastic constants, bulk modulus, and shear modulus of the La-Ce alloys for different Ce/La ratios. Using the quasi-harmonic Debye model, the thermodynamic properties of the La-Ce alloys including the thermal expansion coefficient α and heat capacity C_v are successfully obtained in the temperature range from 0 K to 1000 K. Furthermore, the electronic properties such as density of states and charge densities were also studied.

Key words: Ce-La Alloys; Elastic Properties; Thermodynamics Properties; Density Functional Theory.
PACS numbers: 71.15.Mb; 64.70.kd; 65.40-b; 65.40.De

1. Introduction

Lanthanide metals are well known for their special physical and chemical properties. As the first and second elements of the lanthanides, lanthanum (La) and cerium (Ce) often attract considerable attention. Four structures exist for lanthanum, i.e. body-centered cubic (BCC), face-centered cubic (FCC), hexagonal close-packed (HCP), and double hexagonal close-packed (DHCP) [1], but only FCC and DHCP structures are stable and show superconductivity with the transition temperatures at 6 K and 5 K, respectively [2]. Cerium has f electrons and is one of the few pure elements showing Kondo scattering and isostructural phase transition [3, 4]. It is comparatively easy to obtain Ce-La alloys by melting lanthanum and cerium.

Since the Kondo effect was discovered [5], the study of Kondo systems has attracted great interests. The Ce-La alloy, a perfect Kondo system, has properties, such as the Kondo effect, superconductivity, crystal-field effect, and magnetic susceptibility [6 – 13]. However, few reports exist on its elastic and thermodynamic properties, which are basic physical qualities. Culbert and Edelstein [14] studied the specific heat and entropy of the Ca-Le alloy for cerium concentrations lower than 0.2. They declared that the contribution of magnetism to the specific heat of the Ce-La alloy showed a broad anomaly at 1.2 K, and the specific heat was weakly dependent on the cerium concentration. When the applied temperature is very high, the magnetic interaction is much weaker than the thermal interaction; and Ce-La alloys display different thermodynamic properties. Research work on Ce-La alloys has been mainly experimental. For example, Scott et al. [15] studied the Ce-La alloy microstructure by electron backscatter diffraction. Studies of the properties of Ce-La alloys by theoretical simulation are necessary.

In this work, we focus on the structural, elastic, and thermodynamic properties of Ce-La under pres-

sure by first-principles investigations. We apply the quasi-harmonic Debye model [16] to study the thermodynamic properties with the temperature ranging from 0 to 1000 K. A virtual crystal approximation [17, 18] is applied to establish the Ce-La alloy model. The reminder of the paper is organized as follows: the theoretical method and computational details are given in Section 2, the results and discussion are presented in Section 3, and finally, a summary of our work is given in Section 4.

2. Theoretical Method and Computation Details

2.1. Total Energy Electronic Structure Calculations

In the electronic structure calculations, we adopt three pseudo-potentials, i.e. the on-the-fly (OTF) pseudopotential [19], the ultra-soft pseudopotential [20], and the norm-conserving pseudopotential [21], respectively. We use the exchange-correlation potential of the generalized gradient approximation (GGA) proposed by Perdew et al. [22] and a plane wave basis set with an energy cut-off of 650 eV. The Brillouin-zone sampling we used is the $15 \times 15 \times 15$ Monkhorst–Pack mesh [23] one. The self-consistent convergence precision of total energy is $1.0 \cdot 10^{-6}$ eV/atom. These parameters are carefully tested. All the total energy electronic structure calculations are implemented through the CASTEP code. [24, 25]

The pressure–volume relationship can be obtained by fitting the calculated energy–volume $(E-V)$ data to the Vinet equation of state (EOS) [26]

$$\ln\left[\frac{Px^2}{3(1-x)}\right] = \ln B_0 + a(1-x), x = \left(\frac{V}{V_0}\right)^{1/3}, \quad (1)$$

where $V = V(0,T)$ is the zero-pressure equilibrium volume, derived by integrating the thermodynamic definition of the thermal expansion coefficient $\alpha(T) = V^{-1}\partial V/\partial T$, that is

$$V(0,T) = V(0,0)\exp\int_0^T \alpha(T)\,\mathrm{d}T, \quad (2)$$

where B_0 and $a(=3(B_0'-1)/2)$ are the fitting parameters. $B_T(P,T)$, $B_T'(P,T)$, and $B_T''(P,T)$ are given by

$$B_T = -x^2 B_0 \mathrm{e}^{\alpha(1-x)} f(x), \quad (3)$$

$$B_T' = \left(\frac{\partial B_T}{\partial P}\right)_T = \frac{1}{3}\left[(ax+2) - x\frac{f'(x)}{f(x)}\right], \quad (4)$$

$$B_T'' = \left(\frac{\partial^2 B_T}{\partial P^2}\right)_T = \frac{x}{9B_T}\left\{x\frac{f''(x)}{f(x)} - a + \frac{f'(x)}{f(x)}\left[1 - x\frac{f''(x)}{f(x)}\right]\right\}, \quad (5)$$

where $f(x) = x - 2 - ax(1-x)$.

2.2. Elastic Properties

To calculate the elastic constants under hydrostatic pressure P, we use the symmetry-dependent strains that are non-volume conserving. The elastic constants C_{ijkl} with respect to the finite strain variables are defined as

$$C_{ijkl} = \left(\frac{\partial \sigma_{ij}(x)}{\partial e_{kl}}\right)_X, \quad (6)$$

where σ_{ij} and e_{kl} are the applied stress and Eulerian strain tensors, X and x are the coordinates before and after deformation, respectively. Under pressure P, we have

$$C_{ijkl} = c_{ijkl} + \frac{P}{2}(2\delta_{ij}\delta_{kl} - \delta_{il}\delta_{jk} - \delta_{ik}\delta_{jl}), \quad (7)$$

where c_{ijkl} denotes the second-order derivatives with respect to the infinitesimal strain (Eulerian), and δ is the finite strain variable. The fourth-rank tensor C generally greatly reduces when taking into account the symmetry of the crystal. In a cubic crystal, it is reduces to three components, i.e. C_{11}, C_{12}, and C_{44}.

The bulk modulus B and the shear modulus G of the Ce-La alloy are taken as [27]

$$B = (C_{11} + 2C_{12})/3, \quad G = (G_\mathrm{V} + G_\mathrm{R})/2, \quad (8)$$

where $G_\mathrm{V} = (2c + 3C_{44})/5$, $G_\mathrm{R} = 15 \times (6/c + 9/C_{44})^{-1}$, $c = (C_{11} - C_{12})/2$. G_V is the Voigt shear modulus and G_R is the Reuss shear modulus. The Young modulus E and Poisson ratio σ are related to the hardness of materials, which are given by [28]

$$E = \frac{9BG}{3B+G}, \quad \sigma = \frac{1}{2}\left(\frac{3B-E}{3B}\right). \quad (9)$$

The elastic Debye temperature Θ_E may be estimated from the average sound velocity V_m [29]

$$\Theta_\mathrm{E} = \frac{h}{k}\left[\frac{3n}{4\pi}\left(\frac{N_\mathrm{A}\rho}{M}\right)\right]^{1/3} V_m, \quad (10)$$

where h is Planck's constants, k Boltzmann's constant, N_A Avogadro's number, n the number of atoms per formula unit, M the molecular mass per formula unit, ρ the density, and V_m is obtained from [29] as

$$V_m = \left[\frac{1}{3}\left(\frac{2}{V_S^3} + \frac{1}{V_L^3}\right)\right]^{-1/3}, \tag{11}$$

where V_S and V_L are the shear and longitudinal sound velocities, respectively. The probable values of the average shear and longitudinal sound velocities can be calculated from Navier's equations as follows [30]:

$$V_S = \sqrt{\frac{G}{\rho}}, \quad V_L = \sqrt{\frac{(B + \frac{4}{3}G)}{\rho}}. \tag{12}$$

The Kleinmann parameter is an important parameter describing the relative position of the cation and anion sub-lattices. It is given by the following relation [31]:

$$\zeta = \frac{C_{11} + 8C_{12}}{7C_{11} + 2C_{12}}. \tag{13}$$

2.3. Thermodynamic Properties

The quasi-harmonic Debye model [32], in which the phononic effect is considered, is applied to investigate successfully the thermodynamic properties of some materials [33–35]. In the quasi-harmonic Debye model, the non-equilibrium Gibbs function $G^*(V;P,T)$ can be written in the form

$$G^*(V;P,T) = E(V) + PV + A_{\mathrm{Vib}}(\Theta_D(V);T), \tag{14}$$

where $E(V)$ is the total energy per formula unit, PV corresponds to the constant hydrostatic pressure condition, $\Theta_D(V)$ is the Debye temperature, and the vibrational Helmholtz free energy A_{Vib} can be written as

$$A_{\mathrm{Vib}}(\Theta_D;T) = nkT\left[\frac{9}{8}\frac{\Theta_D}{T} + 3\ln(1 - e^{-\Theta_D/T}) - D(\Theta_D/T)\right], \tag{15}$$

where $D(\Theta_D/T)$ represents the Debye integral, and n is the number of atoms per formula unit. For an isotropic solid, the Debye temperature Θ_D is expressed by

$$\Theta_D = \frac{\hbar}{k}\left[6\pi^2 V^{1/2} n\right]^{1/3} f(\sigma)\sqrt{\frac{B_S}{M}}, \tag{16}$$

where M is the molecular mass, B_S is the adiabatic bulk modulus, which is approximated by the static compressibility

$$B_S \cong B = V\left\{\frac{d^2E(V)}{dV^2}\right\}. \tag{17}$$

$f(\sigma)$ is given in [32], the Poisson σ is taken from the calculated elastic constants, the non-equilibrium Gibbs function $G^*(V;P,T)$ as a function of $(V;P,T)$ can be minimized with respect to volume V:

$$\left(\frac{\partial G^*(V;P,T)}{\partial V}\right)_{P,T}. \tag{18}$$

By solving (18), one can get the thermal EOS. The isothermal bulk modulus B_T, heat capacity C_V, and the thermal expansion coefficient α are given by [32]:

$$B_T(P,T) = V\left(\frac{\partial^2 G^*(V;P,T)}{\partial V^2}\right)_{P,T}, \tag{19}$$

$$C_V = 3nk_B\left[4D(\Theta_D/T) - \frac{3\Theta_D/T}{e^{\Theta_D/T} - 1}\right], \tag{20}$$

$$\alpha = \frac{\gamma C_V}{B_T V}, \tag{21}$$

where γ is the Grüneisen parameter, which is defined as

$$\gamma = -\frac{d\ln\Theta_D(V)}{d\ln V}. \tag{22}$$

Through the quasi-harmonic Debye model, one can obtain the thermodynamic quantities of Ce-La alloys under high pressure and high temperature.

3. Results and Discussion

3.1. Structure and Equations of States

The Ce-La alloy has a face-centered cubic structure with space group *FM-3M*. To assure the accuracy of calculations, we optimized the β-La (FCC) and α-Ce (FCC). We used a series of lattice constants to calculate the total energy E and the corresponding primitive cell volume V. For each lattice constant a, we calculated its V and then obtained the $E-V$ curve. By fitting the calculated $E-V$ data to the Vinet EOS, the bulk modulus B_0 and primitive cell volume V_0 at $P = 0$ and $T = 0$ can be obtained. The equilibrium structure parameters and bulk modulus obtained are listed in Table 1. Our

Table 1. Structure parameters V_0 (Ångström^3) and B_0 (GPa) for pure α-Ce and β-La.

		Present	Experiments	Other calculations
$\alpha-$Ce	V_0	28.88[a] 28.88[b] 26.85[c]	28.06 [4], 29.0 [36], 29.0 [37]	27.07 [3], 24.7 [38]
	B_0	22.11[a] 22.11[b] 37.94[c]	20 [36], 35.0 [39]	41.72 [3], 48.4 [38], 69.4 [40], 37 [41]
$\beta-$La	V_0	37.38[a] 39.68[b] 24.24[c]	37.43 [42]	36.80 [44], 38.28 [2], 38.07 [45]
	B_0	25.88[a] 28.49[b] 29.30[c]	24.80 [33]	24.69 [34], 25.70 [2], 26.59 [35]

[a] Obtained by OTF pseudopotential; [b] Obtained by ultrasoft pseudopotential; [c] Obtained by norm-conserving pseudopotential.

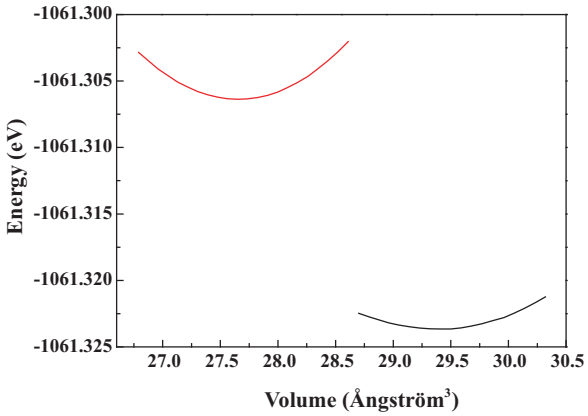

Fig. 1 (colour online). Energy as a function of primitive unit cell volume of cerium.

results from OTF pseudo-potentials agree well with experimental data [4, 36–42]. We noticed that the experimentally determined values for the bulk modulus B_0 of α-Ce are experimental data of 20 and 35 GPa [39]. The discrepancy between the two experimental values of bulk modulus B_0, can be explained further from the $E-V$ curve in Figure 1. When the lattice constant a changes from 4.7 to 5 , we obtained two minimum values of energy. For the latter minimum value, we listed the results obtained in Table 1. For the frontal value, we obtained a calculated result of 32 GPa for the bulk modulus B_0, which is consistent with the experimental values [39]. We found that the frontal minimum value is higher than the latter from Figure 1 and calculated that the frontal minimum value corresponds to a metastable state and the latter corresponds to a stable state of cerium [43]. Our results from the ultra-soft pseudopotential and norm-conserving pseudopotential are unsatisfactory when compared with the experimental data. Therefore, we adopted the OTF pseudopotential in successive calculations.

In Figure 2, we plotted the change in volume V and modulus B_0 as a function of concentration x of cerium. When x increases, the volume decreases gradually. The volume decreases rapidly for small x and slowly for large values of x. We have plotted the lattice constant of the Ce-La alloy as a function of cerium concentration in Figure 3, showing that with increasing cerium concentration, the lattice constants of the Ce-La alloy decrease gradually. With increasing concentration x of cerium, the bulk modulus B_0 increases first, reaches a maximum of 36.9 GPa at $x = 0.5$ and then decreases. By fitting the $B-x$ and $V-x$ data to a fourth-order polynomial, we obtain the following relationships:

$$V_0 = 37.38 + 1.81x - 57.88x^2 + 77.65x^3 - 30.08x^4 , \quad (23)$$

$$B_0 = 25.88 - 1.88x + 176.19x^2 - 334.99x^3 + 156.91x^4 . \quad (24)$$

3.2. Elastic Properties

In Table 2, we present our calculated elastic constants (C_{11}, C_{12}, C_{44}), bulk modulus B_0, and shear modulus G of the Ce-La alloy at different Ce/La ratios under pressure. The elastic constant C_{11} represents the elasticity in length, while C_{12} and C_{44} are related to the elasticity in shape. The elastic constants C_{11} and C_{12} increase at first and then decrease gradually with increasing concentration of cerium, however, C_{44} fluctuates when the pressure reaches 20 GPa for different cerium concentrations. All three elastic constants increase almost linearly with increase in pressure.

The mechanical stability conditions in the cubic structure can be expressed as $\tilde{C}_{44} > 0$, $\tilde{C}_{11} > |\tilde{C}_{12}|$,

Table 2. Elastic constants C_{ij} (GPa), bulk modulus B (GPa), shear modulus G (GPa) for Ce_xLa_{1-x} .

P		0	5	10	15	20	25	30
La	C_{11}	39.38	44.88	58.64	66.85	119.74	158.34	188.30
	C_{12}	18.05	29.49	49.40	53.84	57.52	59.50	67.58
	C_{44}	21.67	15.86	15.73	18.62	53.64	102.14	145.30
	B	25.16	34.62	52.48	58.17	84.99	92.45	101.11
	G	16.31	11.87	9.65	12.22	40.16	76.32	105.46
$Ce_{0.25}La_{0.75}$	C_{11}	42.46	65.65	83.14	84.14	91.62	102.70	137.43
	C_{12}	25.89	35.57	49.02	67.95	81.85	81.47	113.30
	C_{44}	22.34	37.48	46.89	36.40	31.20	43.99	65.39
	B	31.41	45.60	60.40	73.35	85.11	88.55	121.34
	G	15.02	25.99	31.27	20.13	15.28	25.07	33.84
$Ce_{0.5}La_{0.5}$	C_{11}	54.13	76.07	99.33	100.86	91.31	97.70	106.37
	C_{12}	25.50	32.62	51.50	75.53	85.91	119.23	133.48
	C_{44}	35.84	53.33	67.50	62.71	58.88	68.07	78.64
	B	35.04	47.10	67.44	83.97	87.71	112.05	124.44
	G	24.80	37.20	44.55	33.50	21.36	0.63	−1.20
$Ce_{0.75}La_{0.25}$	C_{11}	57.20	80.30	96.39	96.58	135.69	152.66	174.80
	C_{12}	15.43	29.77	54.71	70.39	102.54	108.99	120.25
	C_{44}	45.17	62.78	75.42	82.69	105.12	125.03	148.04
	B	29.36	46.61	68.61	79.12	113.58	123.54	138.43
	G	33.15	43.58	45.21	40.64	51.59	63.51	76.58
Ce	C_{11}	55.44	102.06	111.86	134.02	140.97	134.95	130.44
	C_{12}	7.66	41.04	56.81	80.38	104.66	125.40	149.21
	C_{44}	41.40	60.82	73.96	90.82	97.33	99.00	108.64
	B	23.59	61.38	75.16	98.26	116.76	128.59	142.96
	G	33.21	46.11	49.78	55.84	50.56	36.22	17.23

$\tilde{C}_{11}+2\tilde{C}_{12}>0$ where $\tilde{C}_{ii}=C_{ii}-P\ (i=1,4)$, and $\tilde{C}_{12}=C_{12}+P$. From our calculations, we found that, for lanthanum at pressure 10 GPa and 15 GPa, $Ce_{0.25}La_{0.75}$, $Ce_{0.5}La_{0.5}$, and $Ce_{0.75}La_{0.25}$ at a pressure higher than 15 GPa, and cerium at 20 GPa, the stability conditions are insufficient, and these alloys are mechanically unstable. The shear modulus G for $Ce_{0.5}La_{0.5}$ at pressure 25 GPa is only 0.63 GPa. When the pressure is 30 GPa, the shear modulus is even a minus value -1.20 GPa. A notable phenomenon exists for lanthanum above 5 GPa: C_{44} reduces to 7.65 GPa than 4 GPa. C_{44} decreases with increasing pressure up

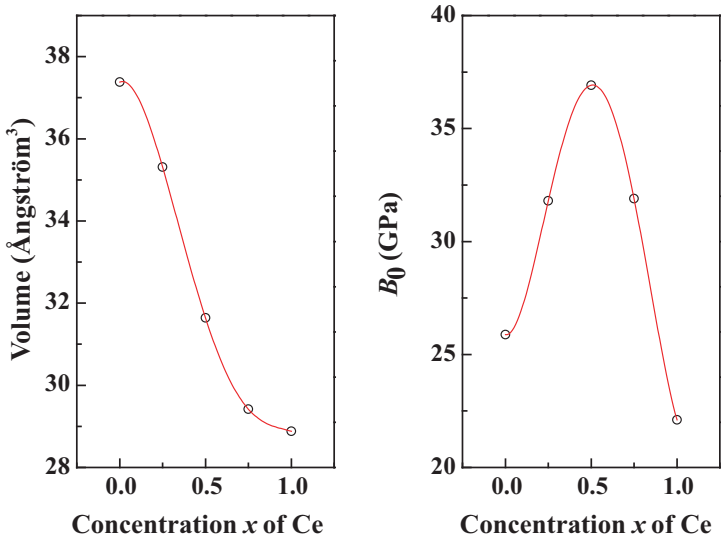

Fig. 2 (colour online). Volume and bulk modulus B_0 of Ce-La alloys as a function of cerium concentration.

P	La	$Ce_{0.25}La_{0.75}$	$Ce_{0.5}La_{0.5}$	$Ce_{0.75}La_{0.25}$	Ce
0	1.54	2.09	1.41	0.89	0.71
5	2.92	1.75	1.27	1.07	1.33
10	5.49	1.93	1.51	1.52	1.51
15	4.76	3.64	2.51	1.95	1.76
20	2.12	5.57	4.11	2.20	2.31
25	1.21	3.53	177.86	1.95	3.55
30	0.96	3.59	−103.70	1.81	8.30

Table 3. Value of B/G (GPa) of Ce-La alloys under pressure (up to 30 GPa).

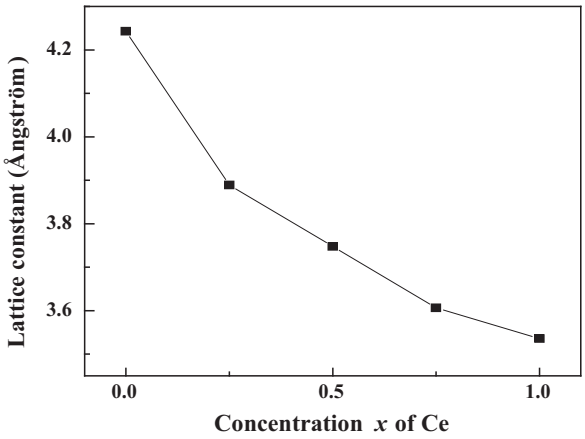

Fig. 3. Lattice constant a of Ce-La alloys as a function of cerium concentration.

to 6.4 GPa. We speculate that there is a phase transition at the pressure 6.4 GPa, which coincides with the experimentally observed second-order phase transition from the FCC structure to the disorted FCC structure [44] at 5.3 GPa and other theoretical result of a second-order phase transition at 4.92 GPa [45].

The bulk or shear modulus can be used to measure the hardness indirectly. From Table 2, it can be seen that the bulk modulus B increases gradually with an increase in pressure, indicating that the Ce-La alloy becomes more difficult to compress with increasing pressure. The critical B/G value, which separates ductile and brittle materials, is approximately 1.75. Table 3 shows the calculated values of B/G at pressures up to 30 GPa. For $Ce_{0.25}La_{0.75}$, this value is greater than 1.75, indicating ductility, while $Ce_{0.75}La_{0.25}$ and cerium change from being brittle to being ductile. For lanthanum, the calculated values of B/G increase with increasing pressure. When the pressure is higher than 15 GPa, the B/G ratio decreases. Results from the mechanical stability and phase transition between 10 and 15 GPa can be used to explain the phenomenon: lanthanum changes to another phase at approximately 15 GPa and leads to a change in B/G.

3.3. Thermodynamic Properties

We analyze the thermodynamic properties of the Ce-La alloy by the quasi-Debye model method. In Figure 4, we present the thermal expansion coefficient α of the Ce-La alloys as a function of temperature. The thermal expansion coefficient α of lanthanum,

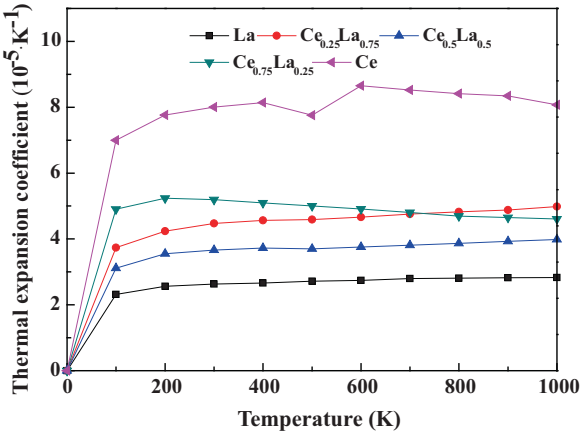

Fig. 4 (colour online). Thermal expansion coefficient of Ce-La alloy as a function of temperature.

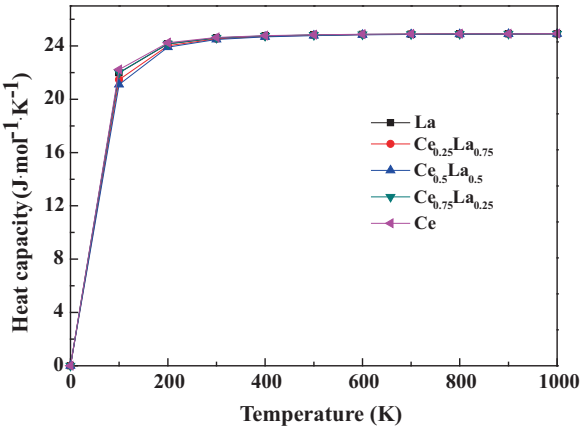

Fig. 5 (colour online). Heat capacity of Ce-La alloys as a function of temperature.

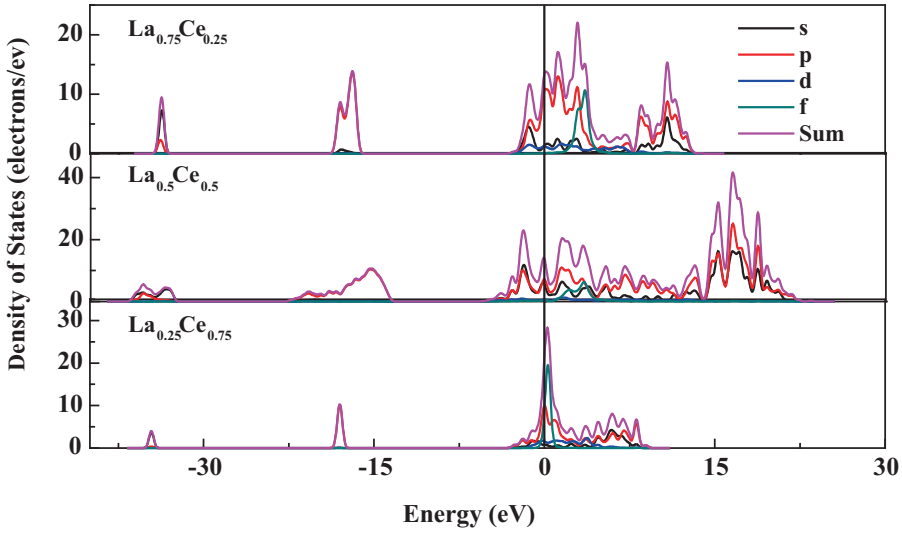

Fig. 6 (colour online). Total and projected density of states densities of Ce-La alloys in different proportions.

$Ce_{0.25}La_{0.75}$, and $Ce_{0.5}La_{0.5}$ changes in a similar manner. When the temperature is below 100 K, the thermal expansion coefficient α increases rapidly with increasing temperature, but increases slowly above 100 K. Therefore, at high temperature, α is not very dependent on the temperature for cerium concentrations below 0.5. $Ce_{0.75}La_{0.25}$ and cerium show different behaviours. The thermal expansion coefficient α of $Ce_{0.75}La_{0.25}$ increases below 200 K and then decreases slowly above 200 K. The thermal expansion coefficient α of cerium has a minimum value at 500 K and decreases slowly above 600 K. The unusual behaviour of the thermal expansion coefficient of cerium may be explained as follows: with increasing concentration of cerium, the strongly correlated effect of the f electron is enhanced and leads to the phenomena observed at approximately 500 K.

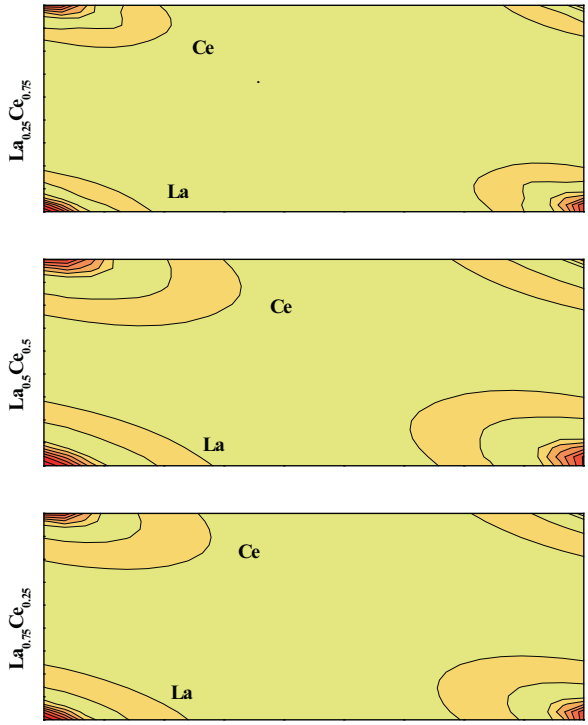

Fig. 7 (colour online). Charge densities of Ce-La alloys in different proportions along (100) plane.

In Figure 5, the variations in heat capacity C_v of the Ce-La alloys with temperature follow Debye's law; at low temperature, C_v is proportional to T^3 and drops rapidly to zero with decreasing temperature. When the temperature is sufficiently high, C_v tends to the Dulong–Petit limit ($C_v(T) \sim 3R$ for monatomic solids). According to virtual crystal approximations, there is only one atom in the primitive cell of the Ce-La alloys, so their Dulong-Petit's limits are $3R = 24.91\ \mathrm{J\,mol^{-1}\,K^{-1}}$.

3.4. Electronic Properties

The density of states plays an important role in the analysis of the physical properties of materials. The total density of state (TDOS) and projected density of state of $La_{0.75}Ce_{0.25}$, $La_{0.5}Ce_{0.5}$, and $La_{0.25}Ce_{0.75}$ are

illustrated in Figure 6. The TDOS value at the Fermi level is not zero, therefore the La-Ce alloys show conductive properties. The peaks of the lower valence bands are located at −35.48 and − 18.38 eV, which are composed predominantly of *s* and *p* states. For alloys $La_{0.75}Ce_{0.25}$ and $La_{0.5}Ce_{0.5}$, the conduction bands are located at − 2.78 eV and are occupied mainly by *s* and *p* states. Above the Fermi level, the conduction bands are dominated by *p* and *f* states and appear as a series of continuous peaks. However, for alloy $La_{0.25}Ce_{0.75}$, there is only a maximum peak coincident with the Fermi energy level. We present the charge densities of the (1 0 0) plane in Figure 7 to understand the nature of the chemical bonding. In Figure 7, the La-Ce bondings at the three concentrations are all anti-bonding states, consistent with our analysis of density of states.

4. Conclusions

We performed first-principles calculations to investigate the structural, elastic, thermodynamic, and electronic properties of La-Ce alloys of different Ce/La ratios. The structural parameters of lanthanum and cerium obtained after relaxation agree favourably with previous work. We calculated the elastic constants and derived the bulk and shear modulus and found that the La-Ce alloys are mechanically stable. The thermodynamic properties including heat capacity and thermal expansion coefficient at high temperatures are predicted using the quasi-harmonic Debye temperature. High temperatures lead to abnormalities in the thermal expansion coefficient of $La_{0.25}Ce_{0.75}$ and cerium. We speculate that this may occur because of the effect of the *f* electrons in cerium. The heat capacity approaches the Dulong–Petit limit at high temperature. The density of states and charge densities along the (100) plane were also obtained. Our results provide useful predictions for a comparison with future experiments.

Acknowledgement

The authors would like to thank the support by the National Natural Science Foundation of China (Grant No. 11204192 and 11104099), the National Key Laboratory Fund for Shock Wave and Detonation Physics Research of the China Academy of Engineering Physics under Grant No. 2012-Zhuan-08, and the Science and Technology Development Foundation of China Academy of Engineering Physics (Grant Nos. 2012A0201007 and 2013B0101002). We also acknowledge the support for the computational resources by the State Key Laboratory of Polymer Materials Engineering of China in Sichuan University.

[1] L. W. Nixon, D. A. Papaconstantopoulos, and M. J. Mehl, Phys. Rev. B **78**, 214510 (2008).
[2] S. Bagc“, H. M. Tütüncü, S. Duman, and G. P. Srivastava, Phys. Rev. B **81**, 144507 (2010).
[3] C. E. Hu, Z. Y. Zeng, L. Zhang, X. R. Chen, and L. C. Cai, Physica B **406**, 669 (2011).
[4] D. C. Koskenmaki and K. A. Gschneidner, Handbook on the Physics and Chemistry of Rare Earths, North-Holland, Amsterdam 1978.
[5] J. Kondo, Prog. Theor. Phys. **32**, 37 (1964).
[6] T. S. Petersen, S. Legvold, K. A. Gschneidner, T. W. E. Tsang, and J. O. Moorman, J. Appl. Phys. **49**, 2115 (1978).
[7] T. S. Petersen, S. Legvold, J. O. Moorman, O. D. McMasters, and K. A. Gschneidner, J. Appl. Phys. **50**, 6363 (1979).
[8] S. DeGennaro and E. Borchi, Phys. Rev. Lett. **30**, 377 (1973).
[9] K. S. Kim and M. B. Maple, Phys. Rev. B **2**, 4696 (1970).
[10] C. Roth, C. Sürgers, and H.v. Löhneysen, Phys. Rev. B **54**, 3454 (1996).
[11] M. B. Maple, J. Wittig, and K. S. Kim, Phys. Rev. Lett. **23**, 1375 (1969).
[12] S. DeGennaro and E. Borchi, Phys. Rev. B **9**, 4985 (1974).
[13] J. J. Wollan and D. K. Finnemore, Phys. Rev. B **4**, 2996 (1971).
[14] H. V. Culbert and A. S. Edelstein, Solid State Commun. **15**, 1633 (1974).
[15] T. B. Scott, C. M. Younes, M. Ling, C. P. Jones, J. A. Nicholson, P. J. Heard, and R. Jenkins, J. Alloy. Comp. **509**, 4284 (2011).
[16] M. A. Blanco, E. Francisco, and V. Luaòa, Comput. Phys. Commun. **158**, 57 (2004).
[17] T. Muto, Sci. Pap. Inst. Phys. Chem. Res. (Jpn.) **34**, 377 (1938).
[18] L. Nørdheim, Ann. Phys. (Leipzig) **9**, 607 (1931).
[19] N. J. Ramer and A. M. Rappe, Phys. Rev. B **62**, 743 (2000).
[20] D. Vanderbilt, Phys. Rev. B **41**, 7892 (1990).
[21] D. R. Hamann, M. Schlüter, and C. Chiang, Phys. Rev. Lett. **43**, 1494 (1979).
[22] J. P. Perdew, K. Burke, and M. Ernzerhof, Phys. Rev. Lett. **77**, 3865 (1996).

[23] H. J. Monkhorst and J. D. Pack, Phys. Rev. B **13**, 5188 (1976).
[24] V. Milman, B. Winkler, J. A. White, C. J. Packard, M. C. Payne, E. V. Akhmatskaya, and R.H. Nobes. Int. J. Quantum. Chem. **77**, 895 (2000).
[25] M. C. Payne, M. P. Teter, D. C. Allen, T. A. Arias, and J. D. Joannopoulos, Rev. Mod. Phys. **64**, 1045 (1992).
[26] P. Vinet, J. H. Rose, J. Ferrante, and J.R. Smith. J. Phys.: Condens. Matter **1**, 1941 (1989).
[27] Z. J. Wu, E. J. Zhao, H. P. Xiang, X. F. Hao, X. J. Liu, and J. Meng, Phy. Rev. B **76**, 054115 (2007).
[28] E. Schreiber, O. L. Anderson, and M. Saga, Elastic Constants and Their Measurement, McGraw-Hill, New York 1973.
[29] O. L. Anderson, J. Phys. Chem. Solids **24**, 909 (1963).
[30] R. Hill, Proc. Soc. London. A **65**, 349 (1952).
[31] W. A. Harrison, Elastic Structure and Properties of Solids, Freeman and Company, San Francisco 1980.
[32] M. A. Blanco, E. Francisco, and V. Luana. Comput. Phys. Commun. **158**, 57 (2004).
[33] H. Z. Guo, X. R. Chen, L. C. Cai, and J. Gao, Solid State Commun. **134**, 787 (2005).
[34] J. Chang, X. R. Chen, W. Zhang, and J. Zhu, Chin. Phys. B **17**, 1377 (2008).
[35] X. R. Chen, Z. Y. Zeng, Z. L. Liu, L. C. Cai, and F. Q. Jing, Phys. Rev. B **83**, 132102 (2011).
[36] J. S. Olsen, L. Gerward, U. Benedict, and J. P. Itié, Physica (Amsterdam) B+C **133**, 129 (1985).
[37] W. H. Zachariasen and F. H. Ellinger, Acta Crystallogr. Sect. A **33**, 155 (1977).
[38] A. Svane, Phys. Rev. B **53**, 4275 (1996).
[39] J. S. Olsen, L. Gerward, J. P. Dancausse, and E. Gering, Physica B **190**, 92 (1993).
[40] L. Huang and C. Chen, J. Phys.: Condens. Matter **19**, 476206 (2007).
[41] P. Söderlind, O. Eriksson, J. M. Wills, and A. M. Boring, Phys. Rev. B **48**, 9306 (1993).
[42] K. Syassen and W. B. Holzapfel, Solid State Commun. **16**, 533 (1975).
[43] J. S. Olsen, L. Gerward, U. Benedict, and J. P. Itié, Physica B+C **133**, 129 (1985).
[44] H. Balter and J. Witting, Low Temp. Phys. **21**, 377 (1975).
[45] G. Y. Gao, Y. L. Niu, T Cui, and L. J. Zhang, J. Phys.: Condens. Matter **19**, 425234 (2007).